AGU ADVANCING EARTH AND SPACE SCIENCE

Geophysical Research Letters

RESEARCH LETTER
10.1029/2020GL090242

Special Section:
Southern Ocean and Climate: Biogeochemical and Physical Fluxes and Processes

Supercooled Southern Ocean Waters

F. Alexander Haumann[1,2], Ruth Moorman[1], Stephen C. Riser[3], Lars H. Smedsrud[4,5,6], Ted Maksym[7], Annie P. S. Wong[3], Earle A. Wilson[8], Robert Drucker[3], Lynne D. Talley[9], Kenneth S. Johnson[10], Robert M. Key[1], and Jorge L. Sarmiento[1]

[1]Atmospheric and Oceanic Sciences Program, Princeton University, Princeton, NJ, USA, [2]British Antarctic Survey, Cambridge, UK, [3]School of Oceanography, University of Washington, Seattle, WA, USA, [4]Geophysical Institute, University of Bergen, Bergen, Norway, [5]Bjerknes Centre for Climate Research, Bergen, Norway, [6]University Centre in Svalbard, Longyearbyen, Svalbard, [7]Department of Applied Ocean Physics and Engineering, Woods Hole Oceanographic Institution, Woods Hole, MA, USA, [8]Environmental Sciences and Engineering, California Institute of Technology, Pasadena, CA, USA, [9]Scripps Institution of Oceanography, University of California, San Diego, La Jolla, CA, USA, [10]Monterey Bay Aquarium Research Institute, Moss Landing, CA, USA

Abstract In cold polar waters, temperatures sometimes drop below the freezing point, a process referred to as supercooling. However, observational challenges in polar regions limit our understanding of the spatial and temporal extent of this phenomenon. We here provide observational evidence that supercooled waters are much more widespread in the seasonally ice-covered Southern Ocean than previously reported. In 5.8% of all analyzed hydrographic profiles south of 55°S, we find temperatures below the surface freezing point ("potential" supercooling), and half of these have temperatures below the local freezing point ("in situ" supercooling). Their occurrence doubles when neglecting measurement uncertainties. We attribute deep coastal-ocean supercooling to melting of Antarctic ice shelves and surface-induced supercooling in the seasonal sea-ice region to wintertime sea-ice formation. The latter supercooling type can extend down to the permanent pycnocline due to convective sinking plumes—an important mechanism for vertical tracer transport and water-mass structure in the polar ocean.

Plain Language Summary Ocean water, which contains about 34 grams of salt per kilogram of seawater, generally freezes around −1.85°C. However, seawater can be cooled to even lower temperatures without turning into ice. This phenomenon is called supercooling. Supercooled water is found in the polar oceans, typically in regions where the ocean is in contact with ice, as is the case for the enormous seasonal sea-ice region around Antarctica. But collecting measurements in this region under the thick ice cover during the dark and cold Antarctic winter is challenging. Here, we supplement rather sparse traditional ship-based observations with data collected by autonomous floats and instrumented marine mammals to detect and analyze where, when, and how supercooled seawater forms in the Southern Ocean. We find widespread supercooling related to melting floating glaciers (ice shelves) along the Antarctic coast and sea-ice formation. Our analysis enables us to detect sinking supercooled plumes from sea-ice formation, which may be important for cooling the deep ocean and transporting constituents such as carbon, nutrients, or oxygen from the ocean's surface to deeper layers.

Key Points:
- Potential and in situ supercooling occurs in large parts of the Southern Ocean seasonal sea-ice zone
- Deep coastal supercooling from below 100 m to the ocean bottom is associated with melting ice shelves and dense shelf water formation
- Shallow supercooling is associated with sea-ice formation and can penetrate as deep as the permanent pycnocline

Supporting Information:
- Supporting Information S1

Correspondence to:
F. A. Haumann,
alexander.haumann@gmail.com

Citation:
Haumann, F. A., Moorman, R., Riser, S. C., Smedsrud, L. H., Maksym, T., Wong, A. P. S., et al. (2020). Supercooled Southern Ocean waters. *Geophysical Research Letters*, *47*, e2020GL090242. https://doi.org/10.1029/2020GL090242

Received 7 AUG 2020
Accepted 26 SEP 2020
Accepted article online 9 OCT 2020

1. Introduction

Supercooled water, that is, water with a temperature below a reference freezing point temperature, has been observed in the polar oceans of the Arctic (e.g., Drucker et al., 2003; Katlein et al., 2020; Skogseth et al., 2009) and Antarctic (e.g., Brett et al., 2020; Countryman, 1970; Lewis & Perkin, 1986). Seawater may be supercooled relative to the local freezing point, making it "in situ" supercooled (Ushio & Wakatsuchi, 1993), or the surface ocean freezing point, making it "potentially" supercooled (Shcherbina et al., 2004). Despite scattered observational evidence of both in situ and potentially supercooled waters in polar oceans, extensive temporal and spatial surveys have been difficult to conduct due to the harsh environmental conditions under which these low temperatures occur. Hydrographic data collected by autonomous profiling floats with an ice-avoidance algorithm (Riser et al., 2018; Wong & Riser, 2011) and instrumented marine animals (Roquet et al., 2013, 2014; Treasure et al., 2017) provide an opportunity to detect supercooled waters year-round (supporting information Figure S1). Using these data to supplement traditional ship-based

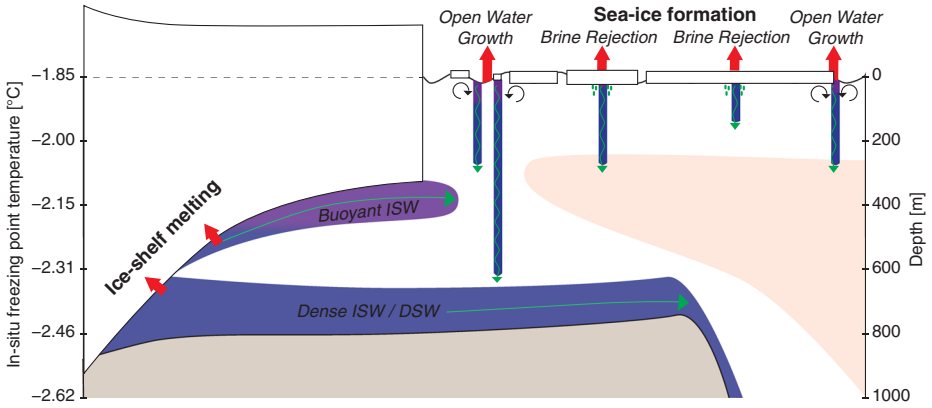

Figure 1. Schematic illustration of processes causing potential (blue shading) and in situ (purple shading) supercooling in the Southern Ocean. On the left: ice-shelf melting forming Ice Shelf Water (ISW) that can either sink as Dense Shelf Water (DSW) or buoyantly rise toward the surface to become in situ supercooled. On the right: sinking supercooled plumes associated with sea-ice formation either caused by turbulent heat loss in open water or by sinking brine. Red arrows illustrate heat loss. Light red shading indicates warm Circumpolar Deep Water. The vertical axes show a decreasing in situ freezing point with depth for a salinity of 34 PSU.

observations, we here analyze the spatial extent and seasonal evolution of supercooled water in the Southern Ocean and study its causes.

The occurrence of supercooled seawater has generally been attributed to two processes: (1) the melting of ice shelves at depth and (2) the formation of sea ice at the surface. The first mechanism relies on the inverse dependence of the seawater freezing point temperature on pressure (Figure 1). Pressurized seawater at depth and in contact with ice shelves in cavities loses heat as it melts the ice (Foldvik & Kvinge, 1974; Jacobs et al., 1985). This heat loss may cool the cavity water to temperatures approaching the local freezing point, which is, for example, about −2.16°C at 400-m depth and 34 PSU. Thus, the resulting Ice Shelf Water (ISW) would be potentially supercooled relative to a corresponding surface freezing point of about −1.85°C. Depending on its density, ISW either sinks as potentially supercooled Dense Shelf Water (DSW) and may leave the continental shelf to form Deep Waters and Antarctic Bottom Water (AABW; Foldvik et al., 2004; Narayanan et al., 2019) or rises along the bottom of the ice shelf (Countryman, 1970; Lewis & Perkin, 1986, Figure 1). If ISW plumes rise, their local freezing point may increase above the water temperature due to the decreasing pressure, leading to in situ supercooling. This process is observed, for example, in McMurdo Sound off the Ross Ice Shelf, where in situ supercooled ISW forms platelet ice at the subsurface (Brett et al., 2020; Langhorne et al., 2015; Leonard et al., 2011).

The formation of sea ice at the surface provides a second mechanism for generating supercooled water. This process has been observed in Arctic (Ito et al., 2015; Skogseth et al., 2009) and Ross Sea (Thompson et al., 2020) polynyas during frazil-ice formation under strong surface heat loss and highly turbulent conditions. Similar conditions have been obtained in laboratory (Smedsrud, 2001; Ushio & Wakatsuchi, 1993) and modeling experiments (Omstedt, 1985; Omstedt & Svensson, 1984), showing that in situ supercooling occurs when the sea-ice formation rate does not keep up with the rate of surface heat loss (Figure 1). As these in situ supercooled surface waters sink, they become potentially supercooled. Potential supercooling could also result from downward mixing of frazil ice by strong winds (Matsumura & Ohshima, 2015). Additionally, supercooling is observed in the Arctic under a closed sea-ice cover and calm conditions (Katlein et al., 2020; Peterson, 2018) and is potentially related to the rejection of cold brine from sea ice. Prior to the present study, there had been no evidence of widespread sea ice-induced supercooling or the occurrence of supercooled waters away from the continental shelf in the Southern Ocean. Because of the lower water column stability compared to the Arctic Ocean (Martinson, 1990), surface-induced supercooling in the Southern Ocean could induce vertical instabilities and convective sinking.

In this study, we analyze hydrographic profiles from autonomous floats, marine animals, and shipboard measurements to detect and map supercooled waters across the entire Southern Ocean. We separate instances of supercooling into those associated with ice-shelf melt and sea-ice growth based on their

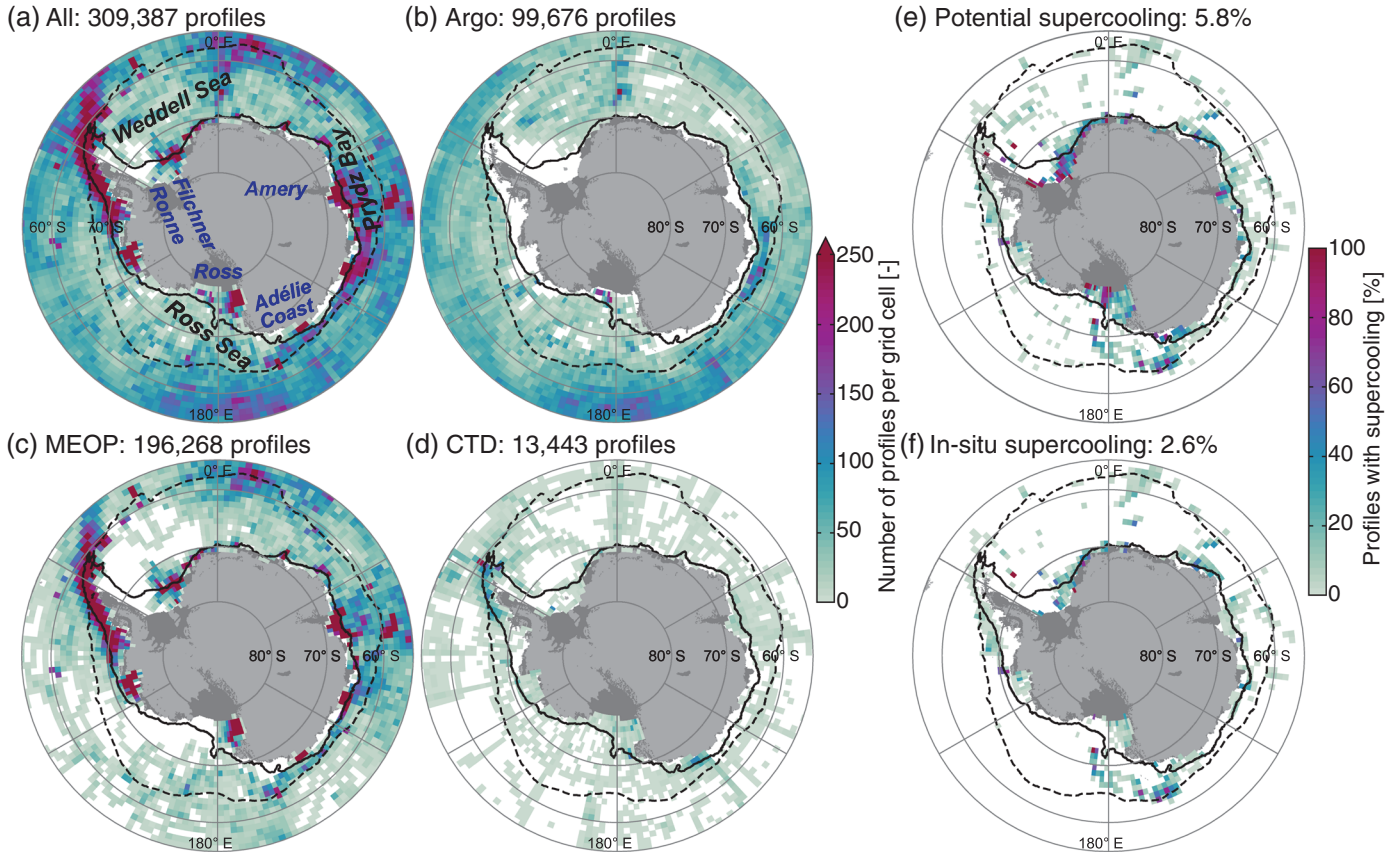

Figure 2. Spatial distribution of (a–d) observations and (e, f) supercooled water in the Southern Ocean. Profiles were mapped on a 2° longitude by 1° latitude spatial grid from (a) all sources, (b) Argo floats, (c) marine mammals, and (d) ship-based measurements. Percentage of all profiles per grid cell that are (e) potentially and (f) in situ supercooled. Black: continental shelf (1,000-m isobath; solid) and climatological mean sea-ice edge (25% ice concentration; dashed).

characteristic properties. Our analysis of the supercooling magnitude, vertical extent, and seasonality provides new insights into the vertical transport of tracers by sinking plumes and the spreading of ISW.

2. Materials and Methods

2.1. Data

For our analysis, we merge temperature, salinity, and pressure data from conductivity-temperature-depth (CTD) profiles collected by three sources: autonomous Argo floats, ship-deployed casts, and instrumented marine mammals. We selected profiles with a "good"-quality flag collected south of 55°S over the period 1972 to 2020, yielding 309,387 profiles in total (Figures 2 and S1). Argo float data (Argo, 2020) have estimated uncertainties in temperature, salinity, and pressure of ±0.002°C, ±0.01 PSU, and ±2.4 dbar, respectively (Wong et al., 2020). Since Argo floats equipped with the ice-avoidance algorithm measure the ocean beneath sea-ice cover but cannot surface through sea ice to transmit their location, we estimate the missing locations by linearly interpolating between the float's prior and subsequent surfacing positions (Chamberlain et al., 2018; Riser et al., 2018). Ship-deployed CTD data stem from the NOAA World Ocean Database 2018 (Boyer et al., 2018, downloaded in NetCDF format 9 June 2020), with estimated uncertainties in temperature, salinity, and pressure of ±0.002°C, ±0.002 PSU, and ±3 dbar, respectively (Hood et al., 2010). Results based on ship data do not change for a possibly larger salinity uncertainty of ±0.006 PSU. Data from instrumented marine mammals stem from the Marine Mammals Exploring the Oceans Pole to Pole (MEOP) consortium (Roquet et al., 2018). After postprocessing, the estimated MEOP uncertainties in temperature and salinity are ±0.02°C and ±0.03 PSU, respectively (Barker & McDougall, 2017; Mensah et al., 2018; Roquet et al., 2011). MEOP profiles are compressed prior to satellite transmission and subsequently reconstructed by linear interpolation, which increases the estimated temperature uncertainty from ±0.02°C to ±0.04°C

(Siegelman et al., 2019). Because we are interested in the minimum temperature of each profile, our analysis is unaffected by this interpolation, and we use the smaller estimated uncertainty. Due to an unknown uncertainty in pressure, we apply the same uncertainty as for ship-deployed sensors (±3 dbar), with our results being robust for a pressure uncertainty of up to ±10 dbar.

Data are retained on their original vertical levels for most of the analysis. However, in order to produce average hydrographic profiles (Figures 4b and 4f), we linearly interpolate all profile data to a 2-m resolution vertical grid and linearly extrapolate profiles to the surface if at least two data points are available in the mixed layer or the upper 20 m of the water column. This extrapolation minimizes aliasing of the mean structure associated with missing data at the surface (Figure S2). For statistical binning (e.g., Figures 4c–4d and 4g–4h), we do not interpolate or extrapolate data but normalize the number of supercooled measurements with the total number of measurements per bin to avoid aliasing. When assessing spatial patterns, we bin data into a regular 2° longitude by 1° latitude grid (e.g., Figure 2).

Satellite-derived sea-ice concentrations used in this study stem from the merged product distributed through the Climate Data Record (1979 to 2018; Meier, Fetterer, Savoie, et al., 2017; Peng et al., 2013) and the corresponding near-real-time product (2019 to 2020; Meier, Fetterer, & Windnagel, 2017). Sea-ice area changes are estimated according to Schlosser et al. (2018).

2.2. Identification of In Situ and Potential Supercooling

We identify separately in situ and potentially supercooled measurements in the merged CTD data set. We define measurements as "in situ" supercooled (Ushio & Wakatsuchi, 1993) if their in situ temperature is below their derived in situ freezing point, which is determined by the local pressure and salinity, assuming air-free seawater (McDougall et al., 2014). "Potential" supercooling (Shcherbina et al., 2004) is defined as the potential temperature (0 dbar) being below the surface-referenced (0 dbar) freezing point, which is a function of salinity only and corresponds to the freezing point of an air-free water parcel if it was adiabatically lifted to the surface. Thus, if a measurement is "in situ" supercooled, it must, by definition, also be "potentially" supercooled. These calculations are performed using the Gibbs-SeaWater (GSW) Oceanographic Toolbox (McDougall & Barker, 2011). Since the magnitude of the supercooling signal (order 0.001°C to 0.1°C) can in some instances be comparable to the measurement uncertainty, we include the respective uncertainties in temperature, salinity, and pressure from each sampling method (section 2.1) and propagate them to the derived quantities. Profiles with a maximum degree of potential supercooling smaller than the uncertainty are excluded from the analysis (section 4). Additionally, 8.8% of the supercooled profiles are excluded due to other issues, leaving 17,896 profiles with significant potential supercooling, of which 7,897 profiles contain in situ supercooling.

2.3. Separation of Sea-Ice and Ice-Shelf Supercooling

We separate all profiles with potential or in situ supercooling into different categories. First, all profiles where the uppermost potentially supercooled layer occurs above 20 m are classified as "sea-ice" supercooled profiles (9,675 profiles). Second, all profiles where the top of the potentially supercooled layer occurs below 100-m depth and at least 10 m below the uppermost measurement are classified as "ice-shelf" supercooled profiles (7,347 profiles). The "sea-ice" supercooling criterion is motivated by the interpretation that supercooling originates at the surface, while the "ice-shelf" supercooling definition is based on the interpretation that heat must be lost at depth. Our choice of classification criteria is supported by the distinct vertical structures and spatio-temporal characteristics of the two resulting sets of supercooled profiles (section 3). We identify a subset of "sea-ice" supercooled profiles that additionally have one or more subsurface supercooled layers (interrupted by non-supercooled layers) as containing both "sea-ice" and "ice-shelf" supercooling (133 profiles). These profiles are included in both categories for spatial and temporal statistics but excluded from vertical statistics. We also identify "sea-ice" supercooled profiles that have potential supercooling over the entire water column or a maximum degree of supercooling either below the permanent pycnocline or below 100 m (3,430 profiles). Here, the permanent pycnocline is defined as the vertical maximum buoyancy frequency (vertically smoothed using a 5-point running mean) at least 10 m below the mixed-layer depth (MLD) or below 50 m if the MLD could not be computed (Feucher et al., 2019). The MLD is defined as the depth where the surface-referenced potential density exceeds the one closest to 10 m (but not exceeding 20 m) by 0.02 kg m^{-3} (de Boyer Montégut et al., 2004; Wilson et al., 2019). These profiles are treated

separately because subsurface ice-shelf processes additional to the surface sea-ice processes cannot be ruled out. Therefore, these profiles are removed from any vertical statistics of the "sea-ice" supercooled profiles but included in the spatial and seasonal statistics of "sea-ice" supercooling. 1,007 supercooled profiles fall into neither "sea-ice" nor "ice-shelf" category and are excluded from our analysis.

3. Results

Out of the 309,387 profiles that we analyzed, 17,896 (5.8%) have a degree of potential supercooling, and 7,897 (2.6%) a degree of in situ supercooling, larger than the respective measurement uncertainties (Figures 2e and 2f). Profiles containing potential supercooling occur predominantly on the continental shelf and close to large ice shelves of the Ross, Weddell, and Pyrdz embayments but also in other continental shelf regions (Figures 2a and 2e). Further, our analysis reveals a surprisingly large coverage of potential supercooling from the coast to the wintertime sea-ice edge. Almost half of the profiles with potential supercooling also show in situ supercooling (Figure 2f). In situ supercooling has a similar spatial coverage to potential supercooling, except it is less concentrated in coastal waters. While their fraction and spatial patterns might be influenced by spatio-temporal sampling biases, our analysis demonstrates that potential and in situ supercooling are much more widespread in the Southern Ocean than had been found in previous, more regionally limited, observations (sections 1 and 4).

We observe the highest percentages of profiles with potential supercooling (7.7%) during austral fall (March to May), followed by austral winter (June to August; 5.5%), and the lowest percentages during austral spring (September to November; 3.6%) and austral summer (December to February; 3.6%; Figures 3a–3d). While it is present year-round on the continental shelf, in the off-shelf region, the coverage largely follows the seasonal evolution of the sea-ice cover and appears to result from sea-ice formation during austral fall and winter. The seasonal cycle of the percentage of profiles that we defined as "sea-ice" supercooled (section 2.3) follow, with a slight delay, the sea-ice growth and decay, with highest percentages between May and July (Figure 3e). In contrast, the occurrence of "ice-shelf" supercooled profiles peaks in late austral summer and fall (March). Such a seasonal "ice-shelf" signal is consistent with the melting seasonality of, for example, the Fimbul (Hattermann et al., 2012; Smedsrud et al., 2006) and Nivlisen (Lindbäck et al., 2019) ice shelves. Late summer melt peaks of these ice shelves have been linked to warm surface waters. However, the seasonality of warm-water intrusion beneath ice shelves and associated basal melting may differ across shelf regions (Jacobs et al., 1985, 1992; Moorman et al., 2020).

The shallow supercooled profiles associated with sea-ice formation processes (3.2%) cover large parts of the seasonal sea-ice region (Figure 4a). Their mean vertical profile exhibits both potential and in situ supercooling in the upper 50 m of the water column (Figure 4b). However, this vertical structure is strongly influenced by the warmer temperatures at the subsurface in some of the profiles, such that the mean signal is more confined to the surface and less uniform than the component profiles (Figure S2). Therefore, we also calculated the mean degree of supercooling below the surface-referenced (solid) and in situ (dashed) freezing point (Figure 4c), which is zero for a degree of supercooling smaller than the respective measurement uncertainty. 98% of the "sea-ice" profiles have a signal of potential supercooling in the upper 10 m with a mean degree of supercooling of 0.050°C (Figure 4c). Almost all of these profiles also have in situ supercooling in the upper 10 m (error bar at 99.5%), which exceeds the measurement uncertainty only in 78% of the cases. In 31% of all the "sea-ice" profiles, the potential supercooling signal extends below the MLD (dashed line in Figure 4c). In fact, in 23% of all cases, the signal reaches the permanent pycnocline (Figures 4d and S3). In a few cases on the continental shelf (3.7%), it extends even below the permanent pycnocline. This deep vertical extent of "sea-ice" potential supercooling provides evidence for dense and cold convective plumes (section 4).

"Ice-shelf" potentially supercooled profiles (2.4%) are confined to the continental shelf region, with largest relative occurrence along the Ross, Filchner-Ronne, and Amery Ice Shelves (Figure 4e). These signals mostly occur at depth (Figure 4f) with a maximum average degree of supercooling of 0.067°C at 564 m (Figure 4g). Most (68%) "ice-shelf" supercooled profiles are shallower than 600 m. Only 14% of the "ice-shelf" profiles have potential supercooling above 200 m, and in 10% of the cases, it occurs above the permanent pycnocline (Figure 4h). The rather deep signal of potential supercooling in these profiles is largely associated with DSW in the four locations identified as source regions for AABW: the Weddell Sea, Ross Sea, Adélie Coast, and Prydz Bay (Figure 4e; Foldvik et al., 2004; Narayanan et al., 2019). While the "ice-shelf" criteria capture

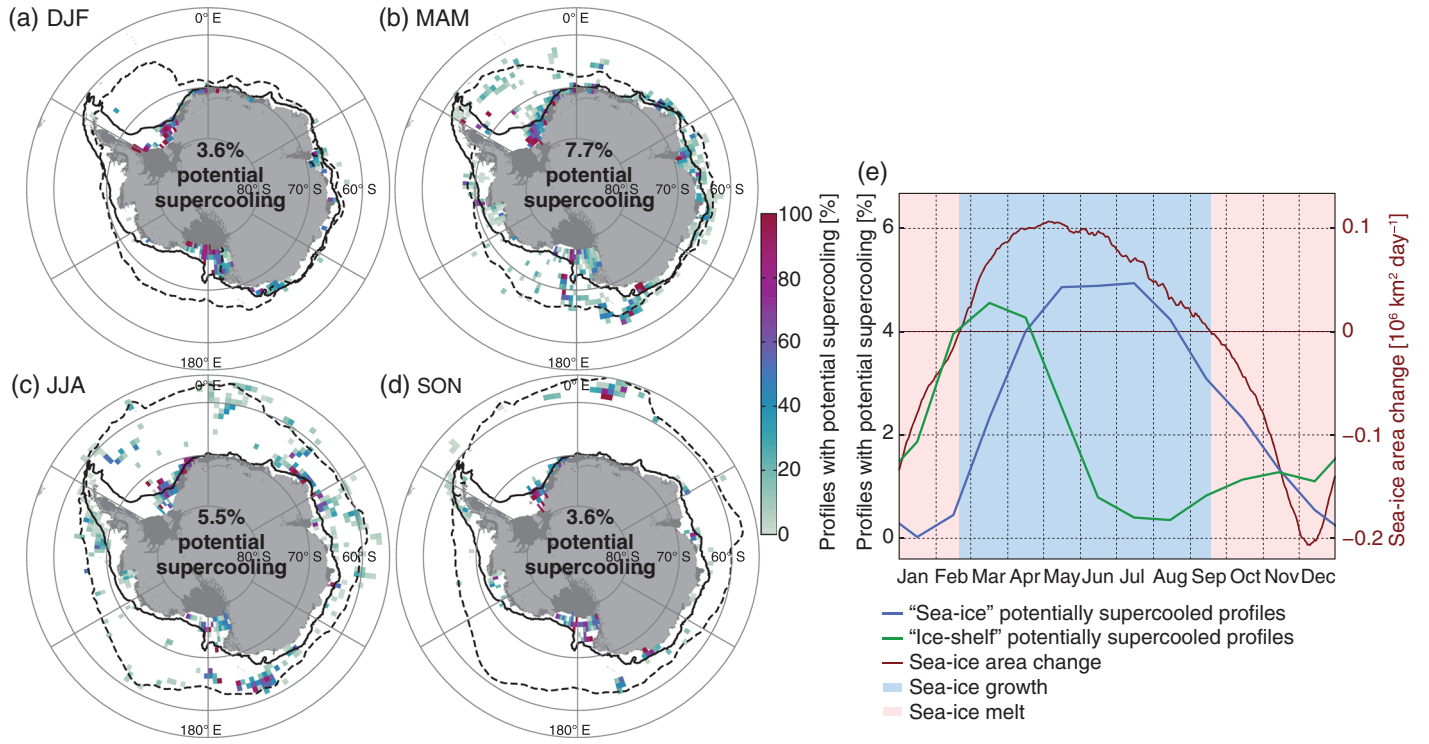

Figure 3. Seasonal evolution of potential supercooling in the Southern Ocean. (a–d) Spatial distribution of profiles with potential supercooling during each season. Black: continental shelf (1,000-m isobath; solid) and climatological mean sea-ice edge (25% ice concentration; dashed). (e) Seasonal cycle of the percentage of all profiles collected south of 55°S that are "sea-ice" (blue) and "ice-shelf" (green) potentially supercooled. Red: climatological daily sea-ice area change. Shading: sea-ice growth (blue) and decay (red).

supercooled water at depth, ISW that rises toward the surface will likely fall into our category characterized by the presence of potential supercooling over the entire water column or a maximum degree of supercooling at depth and at the surface (section 2.3). These profiles occur along ice-shelf edges (Figure S4d) and coincide with previous observations in McMurdo Sound (Brett et al., 2020; Langhorne et al., 2015; Leonard et al., 2011) and Prydz Bay (Penrose et al., 1994).

4. Discussion

Due to the relatively small degree of supercooling (order 0.001°C to 0.1°C), accurate measurements are critical to detect the signals. Accounting for the estimated instrument uncertainty, we find that 44% of all profiles initially identified as potentially supercooled have a maximum degree of potential supercooling smaller than the estimated uncertainty and are excluded from our analysis. Thus, the potential supercooling fraction could be as large as 10.4% (rather than 5.8%) when also including potential supercooling smaller than the instrument uncertainty. Similarly, the in situ supercooling fraction could be as large as 5.9% (rather than 2.6%). Most (98%) of these excluded profiles are from the MEOP data because of their larger uncertainties. The signals stemming from Argo and ship-based data are very robust, but only 10% of the potentially supercooled and 2% of the in situ supercooled profiles stem from these sources. Each of the respective products supports our general finding of a widespread supercooling in the Southern Ocean, but regional patterns might differ due to product specific uncertainties and sampling biases (Figure S5).

Generally, we expect MEOP data to oversample and Argo and ship-based observations to undersample supercooled water. A potential bias in our analysis arises from elephant seals (MEOP) preferentially spending time in leads and polynyas (Labrousse et al., 2018), which would cause an overestimation of the percentage of supercooled profiles, especially those associated with sea-ice formation. This sampling bias could also cause spatial patches of higher occurrences of supercooling (Figures 2e and 2f) where a larger number of MEOP profiles are present (Figure 2c). For example, relatively high supercooling fractions off the Adélie

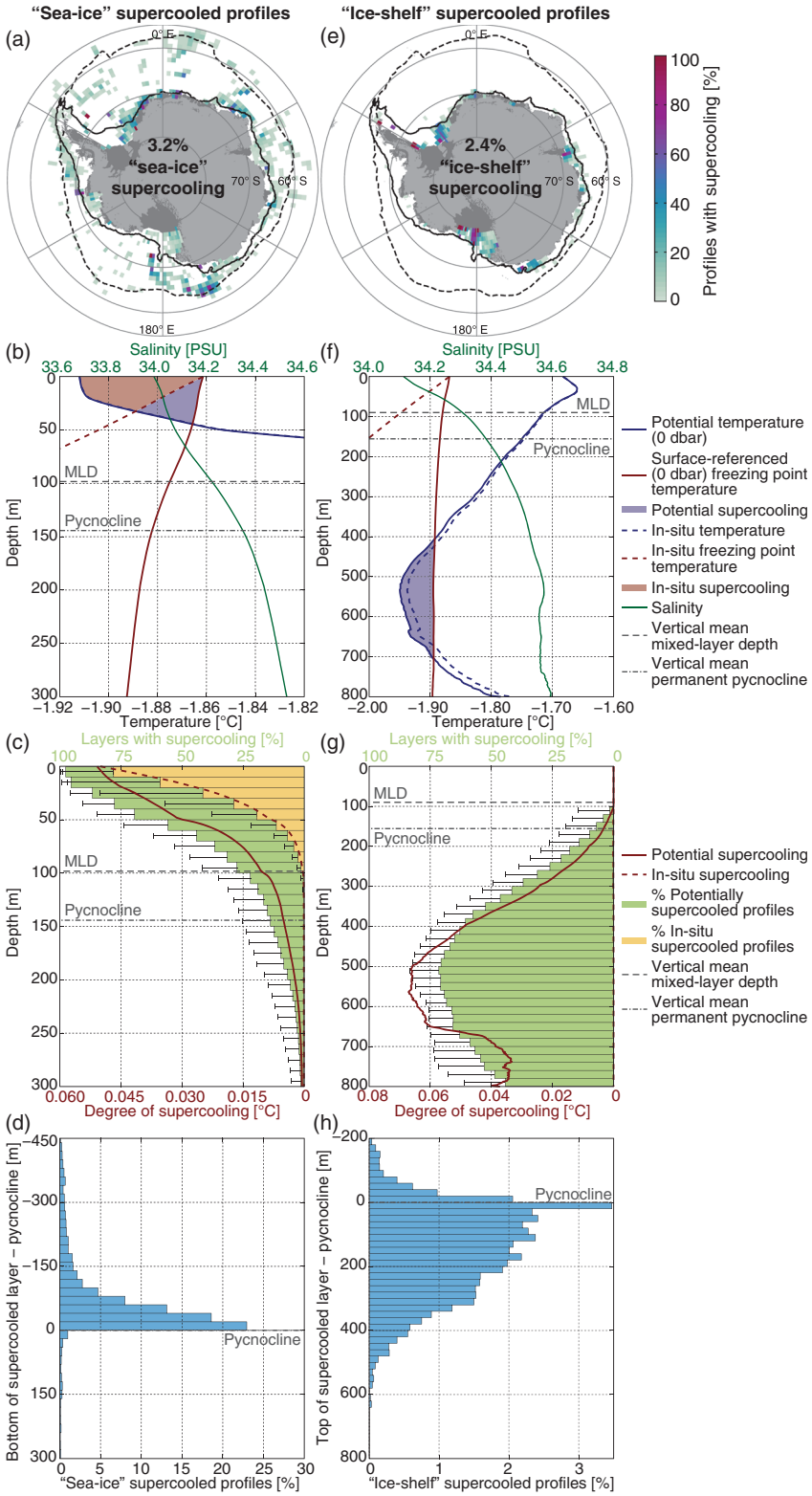

Figure 4. Horizontal and vertical structure of (a–d) "sea-ice" and (e–h) "ice-shelf" supercooled profiles. (a, e) Percentage of profiles per grid cell that are potentially supercooled. Black: continental shelf (1,000-m isobath; solid) and climatological mean sea-ice edge (25% ice concentration; dashed). (b, f) Mean supercooled vertical profiles. (c, g) Mean degree and layer percentage of potential and in situ supercooling. Error bars indicate the respective detection uncertainty due to measurement uncertainties. (d, h) Difference between the (d) bottom (h) top of the supercooled layer and the depth of the permanent pycnocline.

Coast (Figures 2e and 2f) result from a small number of seals with a large number of profiles in certain locations along the sea-ice edge. Another potential overestimation is induced by the large number of profiles concentrated near the Antarctic coast. However, the dominant seasonal signals in Figure 3 are reproduced when the analysis is limited to coastal profiles (Figure S6). Both Argo and ship-based casts might systematically undersample supercooling. Argo floats mostly sample the off-shelf region, which has a generally lower fraction of supercooled profiles (Figure S5a). Additionally, shallow supercooling in winter might be missed by the Argo profiles due to the ice-avoidance algorithm, which causes a termination of the profiles between about 5 and 25 m under ice (Riser et al., 2018) and could thus explain the low fraction of in situ supercooling in Argo data (Figure S5d). The summer bias of ship-based observations causes a lack of detection of "sea-ice" supercooled profiles (Figures S5c and S5f). Due to these issues with the respective data sets, the reported fractions should not be extrapolated to the Southern Ocean as a whole and regional patterns might be affected by sampling biases.

The average monthly mean heat loss required to cause temperatures below the surface freezing point is 6 $W\,m^{-2}$ for the "sea-ice" profiles and 15 $W\,m^{-2}$ for the "ice-shelf" profiles. The heat loss required to form the mean "sea-ice" supercooled layer is equivalent to about 5 cm of sea-ice formation, which seems rather small compared to the several meters of ice that are formed in Antarctic coastal polynyas (Tamura et al., 2016). However, it appears relatively important when considering that the supercooled layer acts to cool the subsurface where heat loss, in the absence of convective plumes, largely occurs through upward vertical diffusion. For example, the annual mean heat loss from Weddell Sea Deep Water to the surface and the atmosphere is estimated to be 16 $W\,m^{-2}$ (Gordon & Huber, 1990). Compared to this heat loss, sinking of supercooled plumes could be an important pathway for extracting heat from the deeper layers of the Southern Ocean that is currently unrepresented in global climate models, which prohibit sustained in situ supercooling.

Further research is needed to investigate the exact causes of the "sea-ice" supercooled profiles. The strong heat loss during winter in wind-induced polynyas, leads, and at the ice edge (Ito et al., 2015; Skogseth et al., 2009), potentially accompanied by turbulent downward mixing of frazil ice (Matsumura & Ohshima, 2015), as well as brine rejection and drainage (Peterson, 2018; Weeks & Ackley, 1982) could contribute. The latter aspect could explain open-ocean supercooling away from major sea-ice formation sites and also during melt season. Brine often forms pockets and channels within the sea ice and is only rejected to the ocean after ice formation (Cole & Shapiro, 1998; Lake & Lewis, 1970). Due to its much higher salinity, the brine has a much lower freezing point temperature than the seawater and thus may be cooler than the freezing point of the ambient water. Under calm conditions, the drainage of cold brine streamers (Middleton et al., 2016; Ushio & Wakatsuchi, 1993) could supercool the surrounding seawater and may lead to the formation of stalactites (Dayton & Martin, 1971; Martin, 1974; Paige, 1970). Supercooling also occurs at a growing sea-ice interface (Weeks & Ackley, 1982), but there have been no studies that suggest that this supercooling can mix deeper and persist. Independent of the question of whether the "sea-ice" supercooled water is associated with turbulent heat loss in the upper layer, downward mixing of frazil ice, or possibly sinking brine, the rather deep-reaching extent of the supercooled layer requires some form convective sinking of dense supercooled plumes from the surface layer. Another potential source of supercooling that we have not considered here and is not well understood is the melting of icebergs in the Southern Ocean. Since melting of icebergs occurs at depth (FitzMaurice et al., 2017), their melt plumes could contain a signal similar to melting ice shelves.

5. Summary and Conclusions

In this study, we show that potential and in situ supercooling is widespread in the Southern Ocean. We find that 5.8% of all analyzed hydrographic profiles south of 55°S carry a signal of potential supercooling and 2.6% of all profiles carry a signal of in situ supercooling. This occurrence is potentially affected by sampling biases and is calculated with a supercooling exceeding the measurement uncertainty. If these criteria are relaxed, 10.4% of profiles have potential supercooling, and 5.9% have in situ supercooling. We identify two distinctly different categories of supercooled profiles, one where the supercooling originates at depth and one where supercooling is induced at the surface. We attribute the former category to the melting of ice shelves along the Antarctic coast and the latter to the formation of sea ice. Both the spatial distribution and seasonal evolution support this interpretation, with the "sea-ice" supercooled profiles following the seasonal expansion

and decay of the sea-ice cover and the "ice-shelf" supercooled profiles occurring along the major Antarctic ice shelves. While supercooled ISW associated with the melting of ice shelves has been studied previously, a widespread occurrence of supercooling associated with sea-ice formation has not yet been identified in the Southern Ocean. We suggest that the "sea ice"-induced potential supercooling can in some cases (23%) reach as deep as the permanent pycnocline due to convective sinking. This rather deep vertical extent of the potential supercooling would extract heat from the subsurface layers, which could be an important process for setting up the Southern Ocean water-mass structure. In addition to vertical heat transport, this process may be important for the vertical transport of salt, carbon, oxygen, and nutrients. Further studies of these processes in the ice-covered Southern Ocean would greatly benefit from suitable measurement platforms, for example, ice-tethered profilers, and technological advances in sensor accuracy and precision.

Data Availability Statement

All data used in this study are openly available in these repositories and cited in the references (https://doi.org/10.17882/42182#72592, https://www.nodc.noaa.gov/OC5/SELECT/dbsearch/dbsearch.html, https://doi.org/10.17882/45461, https://doi.org/10.7265/N59P2ZTG, and https://doi.org/10.7265/N5FF3QJ6). Argo data were collected and made freely available by the International Argo Program and the national programs that contribute to it (http://www.argo.ucsd.edu and http://argo.jcommops.org). The Argo Program is part of the Global Ocean Observing System. The marine mammal data were collected and made freely available by the International MEOP Consortium and the national programs that contribute to it (http://www.meop.net). Ship-based CTD data were made freely available by World Ocean Database 2018 and the national programs that contributed to it.

Acknowledgments

F. A. H. was supported by the Swiss National Science Foundation (SNSF; Schweizerischer Nationalfonds zur Förderung der wissenschaftlichen Forschung) grant numbers P2EZP2_175162 and P400P2_186681. This work was supported by the National Science Foundation (NSF) Southern Ocean Carbon and Climate Observations and Modeling (SOCCOM) Project under the NSF Award PLR-1425989. R. M. would like to thank the National Oceanic and Atmospheric Administration (NOAA) GFDL for mentorship and computational support. S. R. was also supported by the U.S. Argo grant and NOAA grant NA15OAR4320063 to the University of Washington. L. H. S. thanks the Fulbright Foundation for the U.S.-Norway Arctic Chair grant. We are deeply thankful to the large number of scientists, technicians, and funding agencies contributing to these databases, being responsible for the collection and quality control of the high-quality data that form the basis of this work. We thank Josh Plant for his initial notification on very low temperatures observed in some of the float profiles. We would also like to thank the students, teachers, and schools who are participating in the SOCCOM Adopt-a-Float program. Four of the floats used in this study were adopted and have a clear signal of supercooling. These participants are listed in Table S1.

References

Argo (2020). Argo float data and metadata from Global Data Assembly Centre (Argo GDAC)—Snapshot of Argo GDAC of April 9st 2020. SEANOE. https://doi.org/10.17882/42182#72592

Barker, P. M., & McDougall, T. J. (2017). Stabilizing hydrographic profiles with minimal change to the water masses. *Journal of Atmospheric and Oceanic Technology*, *34*(9), 1935–1945. https://doi.org/10.1175/JTECH-D-16-0111.1

Boyer, T. P., Baranova, O. K., Coleman, C., Garcia, H. E., Grodsky, A., Locarnini, R. A., et al. (2018). World Ocean Database 2018. NOAA Atlas NESDIS 87.

Brett, G. M., Irvin, A., Rack, W., Haas, C., Langhorne, P. J., & Leonard, G. H. (2020). Variability in the distribution of fast ice and the sub-ice platelet layer near McMurdo Ice Shelf. *Journal of Geophysical Research: Oceans*, *125*, e2019JC015678. https://doi.org/10.1029/2019JC015678

Chamberlain, P., Talley, L. D., Mazloff, M., Riser, S., Speer, K., Gray, A. R., & Schwartzman, A. (2018). Observing the ice-covered Weddell Gyre with profiling floats: Position uncertainties and correlation statistics. *Journal of Geophysical Research: Oceans*, *123*, 8383–8410. https://doi.org/10.1029/2017JC012990

Cole, D. M., & Shapiro, L. H. (1998). Observations of brine drainage networks and microstructure of first-year sea ice. *Journal of Geophysical Research*, *103*(C10), 21,739–21,750. https://doi.org/10.1029/98JC01264

Countryman, K. A. (1970). An explanation of supercooled waters in the Ross Sea. *Deep-Sea Research and Oceanographic Abstracts*, *17*(1), 85–90. https://doi.org/10.1016/0011-7471(70)90089-6

Dayton, P. K., & Martin, S. (1971). Observations of ice stalactites in McMurdo Sound, Antarctica. *Journal of Geophysical Research*, *76*(6), 1595–1599. https://doi.org/10.1029/JC076i006p01595

de Boyer Montégut, C., Madec, G., Fischer, A. S., Lazar, A., & Iudicone, D. (2004). Mixed layer depth over the global ocean: An examination of profile data and a profile-based climatology. *Journal of Geophysical Research*, *109*, C12003. https://doi.org/10.1029/2004JC002378

Drucker, R., Martin, S., & Moritz, R. (2003). Observations of ice thickness and frazil ice in the St. Lawrence Island polynya from satellite imagery, upward looking sonar, and salinity/temperature moorings. *Journal of Geophysical Research*, *108*(C5), 3149. https://doi.org/10.1029/2001JC001213

Feucher, C., Maze, G., & Mercier, H. (2019). Subtropical mode water and permanent pycnocline properties in the world ocean. *Journal of Geophysical Research: Oceans*, *124*, 1139–1154. https://doi.org/10.1029/2018JC014526

FitzMaurice, A., Cenedese, C., & Straneo, F. (2017). Nonlinear response of iceberg side melting to ocean currents. *Geophysical Research Letters*, *44*, 5637–5644. https://doi.org/10.1002/2017GL073585

Foldvik, A., Gammelsrød, T., Øterhus, S., Fahrbach, E., Rohardt, G., Schröder, M., et al. (2004). Ice shelf water overflow and bottom water formation in the southern Weddell Sea. *Journal of Geophysical Research*, *109*, C02015. https://doi.org/10.1029/2003JC002008

Foldvik, A., & Kvinge, T. (1974). Conditional instability of sea water at the freezing point. *Deep-Sea Research*, *21*(3), 169–174. https://doi.org/10.1016/0011-7471(74)90056-4

Gordon, A. L., & Huber, B. A. (1990). Southern Ocean winter mixed layer. *Journal of Geophysical Research*, *95*(C7), 11655. https://doi.org/10.1029/JC095iC07p11655

Hattermann, T., Nøst, O. A., Lilly, J. M., & Smedsrud, L. H. (2012). Two years of oceanic observations below the Fimbul Ice Shelf, Antarctica. *Geophysical Research Letters*, *39*, L12605. https://doi.org/10.1029/2012GL051012

Hood, E. M., Sabine, C. L., & Sloyan, B. M. (2010). The GO-SHIP repeat hydrography manual: A collection of expert reports and guidelines: IOCCP Report Number 14, ICPO Publication Series Number 134. http://www.go-ship.org/HydroMan.html

Ito, M., Ohshima, K. I., Fukamachi, Y., Simizu, D., Iwamoto, K., Matsumura, Y., et al. (2015). Observations of supercooled water and frazil ice formation in an Arctic coastal polynya from moorings and satellite imagery. *Annals of Glaciology*, *56*(69), 307–314. https://doi.org/10.3189/2015AoG69A839

Jacobs, S. S., Fairbanks, R. G., & Horibe, Y. (1985). Origin and evolution of water masses near the Antarctic continental margin: Evidence from $H_2^{18}O/H_2^{16}O$ ratios in seawater. In S. S. Jacobs (Ed.), *Oceanology of the Antarctic continental shelf* (pp. 59–85). Washington, DC: American Geophysical Union.

Jacobs, S. S., Helmer, H. H., Doake, C. S. M., Jenkins, A., & Frolich, R. M. (1992). Melting of ice shelves and the mass balance of Antarctica. *Journal of Glaciology*, *38*(130), 375–387. https://doi.org/10.3189/s0022143000002252

Katlein, C., Mohrholz, V., Sheikin, I., Itkin, P., Divine, D. V., Stroeve, J., et al. (2020). Platelet ice under Arctic pack ice in winter. *Geophysical Research Letters*, *47*, e2020GL088898. https://doi.org/10.1029/2020GL088898

Labrousse, S., Williams, G., Tamura, T., Bestley, S., Sallée, J.-B., Fraser, A. D., et al. (2018). Coastal polynyas: Winter oases for subadult southern elephant seals in East Antarctica. *Scientific Reports*, *8*(1), 1–15. https://doi.org/10.1038/s41598-018-21388-9

Lake, R. A., & Lewis, E. L. (1970). Salt rejection by sea ice during growth. *Journal of Geophysical Research*, *75*(3), 583–597. https://doi.org/10.1029/JC075i003p00583

Langhorne, P. J., Hughes, K. G., Gough, A. J., Smith, I. J., Williams, M. J. M., Robinson, N. J., et al. (2015). Observed platelet ice distributions in Antarctic sea ice: An index for ocean-ice shelf heat flux. *Geophysical Research Letters*, *42*, 5442–5451. https://doi.org/10.1002/2015GL064508

Leonard, G. H., Langhorne, P. J., Williams, M. J. M., Vennell, R., Purdie, C. R., Dempsey, D. E., et al. (2011). Evolution of supercooling under coastal Antarctic sea ice during winter. *Antarctic Science*, *23*(4), 399–409. https://doi.org/10.1017/S0954102011000265

Lewis, E. L., & Perkin, R. G. (1986). Ice pumps and their rates. *Journal of Geophysical Research*, *91*(C10), 11756. https://doi.org/10.1029/JC091ic10p11756

Lindbäck, K., Moholdt, G., Nicholls, K. W., Hattermann, T., Pratap, B., Thamban, M., & Matsuoka, K.(2019). Spatial and temporal variations in basal melting at Nivlisen ice shelf, East Antarctica, derived from phase-sensitive radars. *The Cryosphere*, *13*(10), 2579–2595. https://doi.org/10.5194/tc-13-2579-2019

Martin, S. (1974). Ice stalactites: Comparison of a laminar flow theory with experiment. *Journal of Fluid Mechanics*, *63*(1), 51–79. https://doi.org/10.1017/S0022112074001017

Martinson, D. G. (1990). Evolution of the Southern Ocean winter mixed layer and sea ice: Open ocean deepwater formation and ventilation. *Journal of Geophysical Research*, *95*(C7), 11641. https://doi.org/10.1029/JC095iC07p11641

Matsumura, Y., & Ohshima, K. I. (2015). Lagrangian modelling of frazil ice in the ocean. *Annals of Glaciology*, *56*(69), 373–382. https://doi.org/10.3189/2015AoG69A657

McDougall, T. J., & Barker, P. M. (2011). Getting started with TEOS-10 and the Gibbs Seawater (GSW) Oceanographic Toolbox. SCOR/IAPSO WG127.

McDougall, T. J., Barker, P. M., Feistel, R., & Galton-Fenzi, B. K. (2014). Melting of ice and sea ice into seawater and frazil ice formation. *Journal of Physical Oceanography*, *44*(7), 1751–1775. https://doi.org/10.1175/JPO-D-13-0253.1

Meier, W. N., Fetterer, F., Savoie, M., Mallory, S., Duerr, R., & Stroeve, J. (2017). NOAA/NSIDC climate data record of passive microwave sea ice concentration, version 3, 1979–2018. NSIDC: National Snow and Ice Data Center, Boulder, Colorado USA. https://doi.org/10.7265/N59P2ZTG

Meier, W. N., Fetterer, F., & Windnagel, A. K. (2017). Near-Real-Time NOAA/NSIDC climate data record of passive microwave sea ice concentration, version 1, 2019–2020. NSIDC: National Snow and Ice Data Center, Boulder, Colorado USA. https://doi.org/10.7265/N5FF3QJ6

Mensah, V., Roquet, F., Siegelman-Charbit, L., Picard, B., Pauthenet, E., & Guinet, C. (2018). A correction for the thermal mass-induced errors of CTD tags mounted on marine mammals. *Journal of Atmospheric and Oceanic Technology*, *35*, 1237–1252. https://doi.org/10.1175/JTECH-D-17-0141.1

Middleton, C. A., Thomas, C., De Wit, A., & Tison, J. L. (2016). Visualizing brine channel development and convective processes during artificial sea-ice growth using Schlieren optical methods. *Journal of Glaciology*, *62*(231), 1–17. https://doi.org/10.1017/jog.2015.1

Moorman, R., Morrison, A. K., & Hogg, A. M. (2020). Thermal responses to Antarctic ice shelf melt in an eddy rich global ocean sea-ice model. *Journal of Climate*, *33*(15), 6599–6620. https://doi.org/10.1175/JCLI-D-19-0846.1

Narayanan, A., Gille, S. T., Mazloff, M. R., & Murali, K. (2019). Water mass characteristics of the Antarctic margins and the production and seasonality of dense shelf water. *Journal of Geophysical Research: Oceans*, *124*, 9277–9294. https://doi.org/10.1029/2018JC014907

Omstedt, A. (1985). On supercooling and ice formation in turbulent sea-water. *Journal of Glaciology*, *31*(109), 263–271. https://doi.org/10.3189/s0022143000006596

Omstedt, A., & Svensson, U. (1984). Modeling supercooling and ice formation in a turbulent Ekman layer. *Journal of Geophysical Research*, *89*(C1), 735. https://doi.org/10.1029/JC089iC01p00735

Paige, R. A. (1970). Stalactite growth beneath sea ice. *Science*, *167*(3915), 171–172. https://doi.org/10.1126/science.167.3915.171-a

Peng, G., Meier, W. N., Scott, D. J., & Savoie, M. H. (2013). A long-term and reproducible passive microwave sea ice concentration data record for climate studies and monitoring. *Earth System Science Data*, *5*(2), 311–318. https://doi.org/10.5194/essd-5-311-2013

Penrose, J. D., Conde, M., & Pauly, T. J. (1994). Acoustic detection of ice crystals in Antarctic waters. *Journal of Geophysical Research*, *99*(C6), 12,573–12,580. https://doi.org/10.1029/93JC03507

Peterson, A. K. (2018). Observations of brine plumes below melting Arctic sea ice. *Ocean Science*, *14*(1), 127–138. https://doi.org/10.5194/os-14-127-2018

Riser, S. C., Swift, D., & Drucker, R. (2018). Profiling floats in SOCCOM: Technical capabilities for studying the Southern Ocean. *Journal of Geophysical Research: Oceans*, *123*, 4055–4073. https://doi.org/10.1002/2017JC013419

Roquet, F., Charrassin, J. B., Marchand, S., Boehme, L., Fedak, M., Reverdin, G., & Guinet, C.(2011). Delayed-mode calibration of hydrographic data obtained from animal-borne satellite relay data loggers. *Journal of Atmospheric and Oceanic Technology*, *28*(6), 787–801. https://doi.org/10.1175/2010JTECHO801.1

Roquet, F., Guinet, C., Charrassin, J.-B., Costa, D. P., Kovacs, K. M., Lydersen, C., et al. (2018). MEOP-CTD in-situ data collection: A Southern Ocean marine-mammals calibrated sea water temperatures and salinities observations. SEANOE. https://doi.org/10.17882/45461

Roquet, F., Williams, G., Hindell, M. A., Harcourt, R., McMahon, C., Guinet, C., et al. (2014). A Southern Indian Ocean database of hydrographic profiles obtained with instrumented elephant seals. https://doi.org/10.1038/sdata.2014.28

Roquet, F., Wunsch, C., Forget, G., Heimbach, P., Guinet, C., Reverdin, G., et al. (2013). Estimates of the Southern Ocean general circulation improved by animal-borne instruments. *Geophysical Research Letters*, *40*, 6176–6180. https://doi.org/10.1002/2013GL058304

Schlosser, E., Haumann, F. A., & Raphael, M. N. (2018). Atmospheric influences on the anomalous 2016 Antarctic sea ice decay. *The Cryosphere*, *12*(3), 1103–1119. https://doi.org/10.5194/tc-12-1103-2018

Shcherbina, A. Y., Talley, L. D., & Rudnick, D. L. (2004). Dense water formation on the northwestern shelf of the Okhotsk Sea: 1. Direct observations of brine rejection. *Journal of Geophysical Research*, *109*, C09S08. https://doi.org/10.1029/2003JC002196

Siegelman, L., Roquet, F., Mensah, V., Rivière, P., Pauthenet, E., Picard, B., & Guinet, C. (2019). Correction and accuracy of high- and low-resolution CTD data from animal-borne instruments. *Journal of Atmospheric and Oceanic Technology*, *36*(5), 745–760. https://doi.org/10.1175/JTECH-D-18-0170.1

Skogseth, R., Nilsen, F., & Smedsrud, L. H. (2009). Supercooled water in an Arctic polynya: Observations and modeling. *Journal of Glaciology*, *55*(189), 43–52. https://doi.org/10.3189/002214309788608840

Smedsrud, L. H. (2001). Frazil-ice entrainment of sediment: Large-tank laboratory experiments. *Journal of Glaciology*, *47*(158), 461–471. https://doi.org/10.3189/172756501781832142

Smedsrud, L. H., Jenkins, A., Holland, D. M., & Nøst, O. A. (2006). Modeling ocean processes below Fimbulisen, Antarctica. *Journal of Geophysical Research*, *111*, C01007. https://doi.org/10.1029/2005JC002915

Tamura, T., Ohshima, K. I., Fraser, A. D., & Williams, G. D. (2016). Sea ice production variability in Antarctic coastal polynyas. *Journal of Geophysical Research: Oceans*, *121*, 2967–2979. https://doi.org/10.1002/2015JC011537

Thompson, L., Smith, M., Thomson, J., Stammerjohn, S., Ackley, S., & Loose, B. (2020). Frazil ice growth and production during katabatic wind events in the Ross Sea, Antarctica. *The Cryosphere*, *14*, 3329–3347. https://doi.org/10.5194/tc-14-3329-2020

Treasure, A., Roquet, F., Ansorge, I., Bester, M., Boehme, L., Bornemann, H., et al. (2017). Marine Mammals exploring the oceans pole to pole: A review of the MEOP Consortium. *Oceanography*, *30*(2), 132–138. https://doi.org/10.5670/oceanog.2017.234

Ushio, S., & Wakatsuchi, M. (1993). A laboratory study on supercooling and frazil ice production processes in winter coastal polynyas. *Journal of Geophysical Research*, *98*(C11), 20,321–20,328. https://doi.org/10.1029/93JC01905

Weeks, W. F., & Ackley, S. F. (1982). The Growth, Structure, and Properties of Sea Ice. In N. Untersteiner (Ed.), *The Geophysics of Sea Ice*, *NATO ASI Series (Series B: Physics)* (pp. 9). Boston, MA: Springer. https://doi.org/10.1007/978-1-4899-5352-0_2

Wilson, E. A., Riser, S. C., Campbell, E. C., & Wong, A. P. S. (2019). Winter upper-ocean stability and ice–ocean feedbacks in the sea ice-covered Southern Ocean. *Journal of Physical Oceanography*, *49*(4), 1099–1117. https://doi.org/10.1175/JPO-D-18-0184.1

Wong, A. P. S., & Riser, S. C. (2011). Profiling float observations of the upper ocean under sea ice off the Wilkes Land coast of Antarctica. *Journal of Physical Oceanography*, *41*(6), 1102–1115. https://doi.org/10.1175/2011JPO4516.1

Wong, A. P. S., Wijffels, S. E., Riser, S. C., Pouliquen, S., Hosoda, S., Roemmich, D., et al. (2020). Argo data 1999–2019: Two million temperature-salinity profiles and subsurface velocity observations from a global array of profiling floats. *Frontiers in Marine Science*, *7*, 700. https://doi.org/10.3389/FMARS.2020.00700